

1
2
3
4
5
6
7
8
9
10
11
12
13
14
15
16
17
18
19
20
21
22
23
24
25
26
27
28

DR. SHIYE ZHAO (Orcid ID : 0000-0003-1559-502X)

Article type : Research Article

Title: Large quantities of small microplastics permeate the surface ocean to abyssal depths in the South Atlantic Gyre

Running title: Microplastics in the ocean's interior

Authors

Shiye Zhao,^{1,2*} Erik R. Zettler,³ Ryan P. Bos,¹ Peigen Lin,⁴ Linda A. Amaral-Zettler,^{3,5,6} Tracy J. Mincer,^{1,7*}

ORCID

Shiye Zhao, <https://orcid.org/0000-0003-1559-502X>

Erik R. Zettler, <https://orcid.org/0000-0002-9266-1142>

Ryan P. Bos, <https://orcid.org/0000-0001-9445-8589>

Peigen Lin, <https://orcid.org/0000-0002-2410-976X>

Linda A. Amaral-Zettler, <https://orcid.org/0000-0003-0807-4744>

Tracy J. Mincer, <https://orcid.org/0000-0002-4644-5609>

Affiliations

¹Harbor Branch Oceanographic Institute, Florida Atlantic University, Fort Pierce, FL 34946, USA

This is the author manuscript accepted for publication and has undergone full peer review but has not been through the copyediting, typesetting, pagination and proofreading process, which may lead to differences between this version and the [Version of Record](#). Please cite this article as [doi: 10.1111/GCB.16089](https://doi.org/10.1111/GCB.16089)

This article is protected by copyright. All rights reserved

29 ²Japan Agency for Marine-Earth Science and Technology, 2-15 Natsushimacho, Yokosuka 237-
30 0061, Japan

31 ³Department of Marine Microbiology and Biogeochemistry, NIOZ Royal Netherlands Institute for
32 Sea Research, Den Burg, Texel, The Netherlands

33 ⁴Woods Hole Oceanographic Institution, Woods Hole MA, USA

34 ⁵Department of Freshwater and Marine Ecology, Institute for Biodiversity and Ecosystem
35 Dynamics, University of Amsterdam, Amsterdam, The Netherlands

36 ⁶The Josephine Bay Paul Center for Comparative Molecular Biology and Evolution, Marine
37 Biological Laboratory, Woods Hole, MA, USA

38 ⁷Department of Biology, Wilkes Honors College, Florida Atlantic University, Jupiter, FL 33458,
39 USA

40 *Corresponding authors: szhao@jamstec.go.jp, tmincer@fau.edu

41

42 **Abstract**

43 Hundreds of studies have surveyed plastic debris in surface ocean gyre and convergence zones,
44 however, comprehensive microplastics (MP, ≤ 5 mm) assessments beneath these surface
45 accumulation areas are lacking. Using *in-situ* high-volume filtration, Manta net and MultiNet
46 sampling, combined with micro-Fourier-transform-infrared imaging, we discovered a high
47 abundance (up to 244.3 pieces per cubic meter [$n\ m^{-3}$]) of small microplastics (SMP,
48 characteristically $<100\ \mu\text{m}$) from the surface to near-sea floor waters of the remote South Atlantic
49 Subtropical Gyre. Large horizontal and vertical variations in the abundances of SMP were
50 observed, displaying inverse vertical trends in some cases. SMP abundances in pump samples
51 were over 2 orders of magnitude higher than large microplastics (LMP, $>300\ \mu\text{m}$) concurrently
52 collected in MultiNet samples. Higher density polymers (e.g., alkyd resins and polyamide)
53 comprised $>65\%$ of the total pump sample count, highlighting a discrepancy between polymer
54 compositions from previous ocean surface-based surveys, typically dominated by buoyant
55 polymers such as polyethylene and polypropylene. Contrary to previous reports stating LMP
56 preferentially accumulated at density gradients, SMP with presumably slower sinking rates are
57 much less influenced by density gradients, thus resulting in a more even vertical distribution in
58 the water column, and potentially longer residence times. Overall, our findings suggest that SMP
59 is a critical and largely underexplored constituent of the oceanic plastic inventory. Additionally,
60 our data support that weak current systems contribute to the formation of SMP hotspots at depth,

61 implying a higher encounter rate for subsurface particle feeders. Our study unveils the prevalence
62 of plastics in the entire water column, highlighting the urgency for more quantification of the
63 deep-ocean MP, particularly the smaller size fraction, to better understand ecosystem exposure
64 and to predict MP fate and impacts.

65 **Key words:** FTIR imaging, *in-situ* pump, microplastics, plastic marine debris, water column,
66 South Atlantic Gyre

68 **Introduction**

69 It has been estimated that between 19 and 23 million metric tons of plastic waste entered the
70 world's aquatic ecosystems in 2016 alone (1). Much of this plastic waste ultimately enters the
71 marine environment, where it is fragmented via physical, chemical and biological processes (2),
72 and subsequently a portion of these plastics are transported across the World Ocean. Currently, up
73 to 51 trillion microplastic (MP) particles are estimated to be floating in the surface waters of the
74 global ocean (3). However, a size-selective loss of MP has been observed at the sea surface (4, 5),
75 suggesting the surface ocean is not the ultimate sink for plastic debris, bringing the ultimate fate
76 of MP into question. Empirical evidence and modelling studies suggest that biological and
77 physical processes of the upper ocean could redistribute MP drifting at sea throughout the pelagic
78 water column (6). A vast majority of plastic marine debris surveys, however, have focused on
79 surface waters (4, 5, 7), and to a lesser extent, deep-sea sediments (8-10).

81 Although the deep sea is Earth's largest ecosystem by volume and area (11), waters below 200 m
82 (12) are just beginning to be explored for MP distributions and include the following: a report by
83 La Daana et al. (13) showed that MP depth profiles ranged from 0-375 n m⁻³ in the Arctic Central
84 Basin, which were analyzed and reported from Niskin bottles collected water samples (7-12 L); a
85 study by Choy et al. (14) employed a large volume (1007-2378 m³ per sample) *in-situ* filtration
86 technique to harvest across epi- and mesopelagic depths to quantify MP abundances (~1.0-15.0 n
87 m⁻³) in Monterey Bay; and a study by Ross et al. found average MP was 37.3 n m⁻³ in Niskin-
88 bottle collected seawater samples (29-67 L) and determined these plastics to be pervasive
89 throughout the water column in the Beaufort Sea (15). Nevertheless, all of these studies were
90 limited to spectroscopic measurements that relied on visual presorting of plastic-like particles and
91 inherently could not reliably include MP <100 μm, a fraction previously demonstrated by other
92 workers to be numerically abundant in the ocean (16, 17). Using micro-Fourier transform infrared
93 (μFTIR) spectroscopic imaging with automated data analysis, Tekman et al. (18) measured MP
94 concentrations from surface waters to deep-sea sediments by filtering >200 L of seawater in the

95 Arctic. The authors unveiled typical concentrations spanning 0-1287 n m⁻³, with MP ≤25 μm
96 accounting for more than 50% of the particle counts in each sample.

97
98 As plastic particles disintegrate into smaller size fractions, they can become harmful in different
99 and unpredictable ways that are only beginning to be understood. For example, MP smaller than
100 150 μm can translocate across the gut epithelium (19), become trapped in biomass, and have the
101 potential to transfer through marine food webs, posing an unknown ecological risk and
102 biogeochemical impacts. The occurrence of these smaller MP in food webs and surrounding
103 seawaters, however, is underreported due to the difficulty of sampling high volumes of water and
104 the need for specialized analytical methods required for characterizing small particles from
105 samples (20).

106
107 The presence of accumulation zones of plastic marine debris located within the five subtropical
108 gyres has been verified (4, 5, 7). These studies all focused on LMP collected via surface-trawl
109 plankton nets and were sorted visually. To date, only two studies have reported the presence of
110 smaller MP (<300 μm) in the surface waters of the North Atlantic Gyre (16, 21). Most recently,
111 11.6-21.1 million tonnes of polyethylene (PE), polypropylene (PP), and polystyrene (PS) MP (32-
112 651 μm) were estimated to be in the top 200 m of the Atlantic Ocean after collection from three
113 discrete depths along a north-south transect with in-situ pumps and μFTIR polymer identification
114 (22); however, this study was limited to only PE, PP and PS, presenting a possible knowledge gap
115 of other plastic polymers (22). Recently, other polymers (e.g., polyamide, polyurethane) rather
116 than PE, PP and PS have been reported to be the dominant plastics of sub-surface marine samples
117 (18, 23). Therefore, a more complete dataset containing all identified polymers is necessary to
118 provide a comprehensive understanding of ocean plastic pollution. It is plausible that small MP
119 are ubiquitous in the deep-ocean waters underneath offshore plastic accumulation zones, based on
120 their high abundances in the upper layer (<200 m) of mid-latitude oceanic gyres mentioned above
121 (16, 21, 22). Furthermore, the observations of open-ocean SMP in the shallow and deep-pelagic
122 waters have only been reported in two studies (18, 22), both of which disclosed the inconsistency
123 of the vertical trends of plastic abundance and distribution across sampling stations. This unclear
124 pattern in vertical profiles of water-column plastics has been attributed to the unknown
125 redistribution and removal processes in the ocean interior (6). A better mechanistic understanding
126 of how plastics sink from the ocean surface beyond the mixed layer and ultimately to abyssal
127 depths is critical to predicting its fate and impacts on the marine ecosystems.

129 In this study we sampled plastic particles in the South Atlantic Subtropical Gyre (SASG, Fig. 1)
130 by deploying a combination of surface Manta nets (*SI Appendix*, Table S1), multiple
131 opening/closing nets at discrete depths in the top 100 m (*SI Appendix*, Table S1), and McLane *in-*
132 *situ* Large Volume Water Transfer System (WTS-LV) pumps at four different stations from
133 surface to near-seafloor depths (*SI Appendix*, Table S2) in the South Atlantic plastic accumulation
134 zone (4). Our combined analysis procedure, including the automated interpretation of spectral
135 datasets created by μ FTIR imaging, provide a more integrative view of the distribution,
136 abundance, dimensions and chemical nature of plastic particles in the interior of an ocean gyre.

137 **Materials and Methods**

138 **Study Area and Sample Collection.** Samples were collected while onboard the RV *Pelagia* cruise
139 64PE-448 during the 21-day long “Sinergia” SASG Cruise (January 4th-24th, 2019). Two stations
140 (A, D) located in the outer accumulation zone of the SASG, and two stations (B, C) located in the
141 inner accumulation zone, were chosen to collect oceanic particle samples in the water column
142 (Fig.1). According to previous model results (4, 5), the outer accumulation zone of the SASG has
143 a modeled average concentration of surface plastics of ~ 100 g per km^2 , while the inner
144 accumulation zone shows a mean concentration of plastics of ~ 600 g per km^2 . Manta net
145 (Oceaninstruments) and MultiNet (Hydro-bios) samples (Fig.1 and S1, Table S1) were collected
146 before deploying the WTS-LV pumps (LV08, McLane Research Laboratories). Four WTS-LV
147 pumps were used in total: three pumps were fitted with three standard radial filter holders and one
148 pump was fitted with a 3-tier filter holder. All filter holders were made of black acetal which we
149 analyzed for our polymer workflow library. The site of deploying the WTS-LV pumps at each
150 station were purposely distant (on average about 5 nautical miles) from the location where the
151 Manta net and MultiNet were retrieved. These intervals assured the prevention of potential
152 contamination of pump samples from the possible shedding of nylon fiber from the mesh material
153 of the Manta net and MultiNet collection devices. For the details of net and pump samplings,
154 please refer to Table S1 and S2. Manta trawls were carried out using a Manta net (0.86 m wide \times
155 0.15 m vertical opening) with a 500 μm mesh net and a closed cod end. The MultiNet had an
156 opening of 0.5 \times 0.5 m, with 200 μm mesh nets and plastic cod ends with 100 μm mesh windows.
157 The Manta nets were towed in a straight line for 30 minutes at 2 knots at each Manta net tow
158 station ($n = 5$, MT-05, -14, -16, -18, -22, Fig.1). The MultiNet samples were collected at five
159 different depths (Table S1). The net was lowered to the maximum depth with all nets closed, then
160 nets were opened/closed individually and towed for 25-48 min at each depth. The net depth was
161 monitored continuously and maintained within 3 m of the target depth, then closed before raising

162 the frame to the next depth. Three MultiNet deployments (MN-01 at depths of 20, 40, 60, 80 100
163 m; both MN-02 and MN-03 at depths of 5, 10, 20, 40, 60 m) were conducted around the WTS-LV
164 pump stations A, B and C (Fig.1, Table S1 and S2). The volume of seawater filtered was
165 determined from the readings of a mechanic flowmeter (2030RC, General Oceanics) within the
166 mouth of the net. Once the net (Manta net or MultiNet) was retrieved from the sea, it was
167 thoroughly rinsed on board with a seawater hose from the outside inwards, from the mouth
168 toward the end to accumulate all the material in the cod-end. Then, the cod-end was removed and
169 rinsed down into a clean bucket. In the onboard laboratory, any plastic-like particles floating in
170 each bucket were picked out visually. Then remaining samples in the bucket were poured onto a
171 300- μm mesh size sieve. Once sieved, the content retained was carefully examined, and plastic-
172 like particles were transferred to the white plastic tray. When in doubt, the particle was checked
173 with the aid of a stereomicroscope and retained for FTIR analysis. Counts were documented for
174 each Manta net and MultiNet sample. Finally, particles were dried and stored in the dark in glass
175 scintillation vials with foil lined caps (20 ml) for polymer analysis (see below).

176
177 At each station, a conductivity-temperature depth (CTD, Sea-Bird Electronics) profile was
178 collected to measure standard parameters (e.g., conductivity, temperature, dissolved oxygen) of
179 the deployment area. Using the profiles of these parameters (Fig. S2), distinct water layers of
180 interest were identified such as the mixed layer, pycnocline, Antarctic Intermediate Water (AAIW)
181 and the Antarctic Bottom Water (AABW). The WTS-LV pumps were tethered to a single wire
182 and deployed at predetermined depths (Fig.S2, Table S2) using a modified pumping method (24).
183 For each pump unit, seawater was directed through a series of filters: The samples passed through
184 stacked pre-combusted 200 and 40 μm stainless steel (SS) mesh screens followed by the pre-
185 combusted 2.0 μm quartz fiber filter (Whatman QM-A). Thus, >200 , 40-200, and 2-40 μm size-
186 fraction particles were retained by the SS and QM-A filters. The effective filtration area of these
187 filters was $\sim 125 \text{ cm}^2$. The reasons for selecting QM-A filters were as follows: 1) quartz fiber
188 filters can be pre-combusted to avoid potential contamination, which is particularly important for
189 studying small microplastic; and, 2) in comparison to membrane filters, QM-A filters have better
190 particle loading and uniformity (24). The disadvantage of using QM-A filters, however, is that its
191 pore tortuosity (a fluid dynamic term for the complex path a particle takes with twists and turns)
192 is better suited for trapping particles at the surface and inside the filter media. However, retaining
193 particles within the filter layers is not conducive to particle extraction and thus probably results in
194 an underestimation of plastic abundances. During particle extraction in this study disintegration of

195 QM-A filters was observed which would release the entrapped particles and improve recovery
196 rate.

197

198 All pumps were programmed to run for five hours and stop if flow rates fell below 3-4 L/minute,
199 resulting in a range of 440 to 1765 L seawater filtered, depending on *in-situ* particle
200 concentrations (Table S2). Of all filters, only QM-A filters, which collected 2-40 μm sized
201 particles, were analyzed in this study. The QM-A filters and SS meshes were folded and wrapped
202 with pre-combusted foil, and immediately stored at $-80\text{ }^{\circ}\text{C}$ until analysis. At the end of the cruise,
203 all filters were transported on dry ice to the laboratory and stored at $-80\text{ }^{\circ}\text{C}$ prior to further
204 processing. Calm seas prevailed during the WTS-LV pump sampling (Table S1).

205

206 ***Extraction of SMP in Pump Samples.*** To isolate SMP, the QMA filters wrapped within the
207 aluminum foil were thawed to room temperature for ~ 3 h under a laminar flow hood. Three
208 subsamples of the QM-A filters from each pump were taken with a flamed metal punch (23 mm
209 diam.) sampling along the surface. Based on the filtration efficiency and filtration area
210 calculations of the QM-A filters, each subsample corresponded to ~ 100 L of filtered seawater and
211 were therefore recognized as one technical replicate. A total of three technical replicates were
212 analyzed for each pump, and the filtered seawater volume of each replicate ranged from 102.3 L
213 to 139.9 L (Table S1). For each replicate, the sub-sampled QM-A filters were placed into separate
214 pre-combusted borosilicate glass scintillation vials (20 ml, DMK, Life Sciences Kimble)
215 containing sodium iodide (NaI : $1.65\text{-}1.70\text{ g cm}^{-3}$) and sonicated for 5 min. These subsamples were
216 then pooled into a 50 ml conical centrifugation tube (DMK, Life Sciences Kimble) and
217 centrifuged at 1600 rpm for 15 minutes. The supernatant was filtered onto a pre-combusted
218 stainless-steel filter ($5\text{ }\mu\text{m}$), and this procedure was repeated at least three times per replicate. The
219 sample on the stainless-steel filter was stored in a scintillation vial with 5 ml 5% potassium
220 hydroxide at $60\text{ }^{\circ}\text{C}$ for 24 hours for removal of organic matter. Potassium hydroxide was
221 neutralized with hydrochloric acid, and particles on the stainless-steel filter were detached by
222 sonication for 5 minutes. Particles in the liquid were concentrated onto an Anodisc filter ($0.2\text{ }\mu\text{m}$
223 pore size, GE Whatman) held in a glass filter holder (Advantec, 13 mm in diameter), followed by
224 a thorough vial rinsing step with 50% ethanol to remove SMP that could possibly adhere to the
225 glass vessel. The rinsing steps was done three times to increase SMP yields. The Anodisc filter
226 was then dried at $37\text{ }^{\circ}\text{C}$ overnight prior to μFTIR analyses.

227

228 To test the influences of the sample storage and experimental steps, aged plastics (n=10) from our
229 Manta net samples were placed into a pre-combusted glass scintillation vial and stored at -80 °C
230 for 3 days. Plastics were subsequently thawed at room temperature for 3 hours and processed
231 following the identical procedure as the samples. The mechanical transformation was evaluated
232 by comparing the geometries (i.e., Feret diameter) and weights of these particles at pre-test to
233 post-test. No apparent changes were found.

234
235 **Polymer Analysis.** SMP particles were identified by μ FTIR spectroscopy (Thermo Scientific™
236 Nicolet™ iN10, USA) in a HEPA filtered laminar flow hood. The entire sample-filter area (13
237 mm in diameter) was mapped using the FTIR microscope in transmission mode using an MCT/A
238 detector (aperture size: 25 μ m \times 25 μ m, 1 scan at 16 cm^{-1} resolution, step size: 21 and 22 μ m).
239 The background position was selected as an area clear of particles on the Anodisc filter. Upon
240 acquiring the FTIR chemical images of samples (more than 17 million individual spectra were
241 generated in total), the particle polymer types were confirmed using two steps (Fig. S3): (Step I)
242 All spectra of the resulting chemical maps were subject to preprocessing with the auto-baseline
243 correction and normalization in OMNIC Picta (Thermo Fisher Scientific, USA). All spectra
244 within the whole chemical map were exported to CSV files and SPA files. Then all the spectra
245 (CSV files) were compared automatically against a transformed reference library (25) with the
246 search algorithm (Pearson's correlation) using a Python script. When Pearson's correlation coeffi-
247 cient between the experimental and the library spectrum was larger than 0.8, the position and
248 polymer types of each identified spectrum were recorded; (Step II) Based on the coordinates,
249 spectra were tracked in chemical maps, and the polymer identity was confirmed by comparing
250 with the Hummel Polymer Sample Library in OMNIC Picta. The software interpretation was
251 systematically validated (>70% match with reference spectra) or rejected (<60% match with
252 reference spectra). Spectra with a match between 60% and 70% were individually reinterpreted
253 by confirming the clear presence of specific polymer peaks. The particle was only verified to be
254 plastic if its spectrum was confirmed as the same polymer type by both steps. Procedure blanks
255 were scanned and analyzed with the same methods.

256
257 To verify the polymer composition in the Manta net samples, the FTIR Spectrometer (Thermo
258 Scientific™ Nicolet™ iN10, USA) in the attenuated total reflection mode in the spectral range
259 from 3600 to 1250 cm^{-1} was applied to selected particles. A total of 33% (n = 457) of the total
260 particles collected in nets (n = 1406) was analyzed. The polymer type of each particle was

261 confirmed by comparing its FTIR spectra against the Hummel Polymer Sample Library in
262 OMNIC Picta. The polymer composition was identified according to the criteria mentioned above.

263
264 **Oxidation Degree.** Plastics are manufactured with different additives (e.g., plasticizers, stabilizers)
265 based on polymer application (e.g., plasticizers, stabilizers) and therefore may differ in their
266 reaction to various levels of environmental exposure to temperature and ultraviolet light.
267 Consequently, plastic debris may exhibit a large variety of degradation signatures. Characterizing
268 weathering degree is critical to better understand the origin and fate of environmental plastics (15).
269 The carbonyl indices have been often used to estimate the weathering degree of plastics in
270 literature (15, 26, 27). Therefore, PE polymers, the most common resin types found in the open
271 ocean, were selected to study oxidation degree by comparing carbonyl indices. The carbonyl
272 indices of PE large microplastics (PE-LMP) in the Manta net samples and the PE small
273 microplastics (PE-SMP) collected by the WTS-LV pumps were calculated by measuring the ratio
274 of the absorbance band area of the carbonyl group at $1630\text{-}1850\text{ cm}^{-1}$ and the olefinic band area at
275 $1420\text{-}1490\text{ cm}^{-1}$ (28, 29). Although little degradation of plastics due to the 10% KOH processing
276 step has been documented (30-32) we took the extra precaution in our study to employ 5% KOH
277 to purify samples and calculated carbonyl index based on two band areas, which differs from
278 previously published methods (two spectral peaks), thus further minimizing the potential artifacts
279 of KOH treatment on FTIR spectra and carbonyl index determination.

280
281 **SMP Characteristics.** The optical images of particles were often partially blurred due to the
282 combination of irregularly shaped particles and the motion of particles during the high-speed
283 imaging (10 steps per second). Therefore, the major (the maximum Ferret's diameter) and the
284 minor axes (the longest axis perpendicular to the major axis) of each SMP were measured on the
285 pseudo-color infrared image according to a method by Simon et al. (33). Briefly, the infrared
286 image of each identified particle was located with the OMNIC Picta depending on its x, y
287 coordinates. Based on the polymer assignment, the infrared image was highlighted in the specific
288 band region of the assigned polymer. Band regions for distinguishing polymer types were
289 provided by Löder et al. (34). Then, all neighbor pixels showing the same polymer assignment
290 were confirmed and recognized as the same particle. By observing the pseudo-color image, the
291 boundary of the particle, which shows significant contrast with the ambient pixels, can be clearly
292 determined (Fig. S3). The particle dimensions were measured with the ruler tool in the OMNIC
293 Picta software. In this study, the uncertainty of plastic size measured on infrared images lies

294 within 5 μm when comparing to particle images obtained in the visible wavelengths. However,
295 such an uncertainty would not cause a significant error in the particle size distribution.

296
297 The aspect ratio of the SMP, a measure of particle shape, can be estimated by calculating the ratio
298 of the minor and major axes. To estimate the mass of the identified plastic particle, each SMP was
299 assumed to be an ellipsoid. Based on the ellipsoid volume model (35), the volume of SMP was
300 calculated using the major (a), minor (b), and intermediate (c) axes:

$$301 \quad V = \frac{\pi abc}{6}, \quad (1)$$

302 The intermediate axis (c) of each SMP was estimated by multiplying the minor axis and the
303 median aspect ratio (0.67 ± 0.12) of all SMP (33). The mass of SMP was calculated from the
304 volume and the density (ρ , Table S5) of the assigned plastic type: $Mass_{MP} = \rho V$. (2).

305 **Theoretical Sinking Rates of SMP.** Because of their small sizes, SMP particles (n=148) in our
306 study, which are heavier than the averaged seawater density of the top 200 m, are characterized
307 by low Reynolds numbers. Therefore, the theoretical sinking velocities (v) of SMP particles
308 composed of polymers denser than the seawater was calculated using the Stokes' formula:

$$309 \quad v = 2(\rho_p - \rho_f)gR^2/9\mu, \quad (3)$$

310
311 where ρ_p is the density of the particles (kg m^{-3} , Table S5). ρ_f is the mean density of the seawater of
312 the top 200 m in our study area (1.026 kg m^{-3}). g is the gravitational field strength (m s^{-2}). R , the
313 radius of the equivalent spherical diameter, was calculated on the basis of a best-fit ellipse used in
314 the formula (1). μ is the dynamic viscosity of seawater ($\sim 10^{-3} \text{ kg m}^{-1} \text{ s}^{-1}$) taken from Ardekani and
315 Stocker (36).

316
317
318 **LMP Data Processing.** All identified polymer particles from the Manta net samples were
319 weighed on an analytical balance. The averaged MP mass per piece was the total weight of
320 plastics divided by the total number and subsequently employed to estimate the plastic mass in
321 both Manta net and MultiNet samples. Because of the wind-induced vertical mixing, MP counts
322 collected by Manta net may underestimate the total number of buoyant plastics in the area
323 sampled (37). Thus, the integrated MP abundance/mass for the top 5 m in our study area was
324 approximated with the equation and parameters used in literature (38,39)

326 **Hydrodynamic data.** The climatology of sea surface height and geostrophic current was
327 computed using the daily data obtained from the Copernicus Marine and Environment Monitoring
328 Service (CMEMS, <http://www.marine.copernicus.eu>). It has a spatial resolution of 0.25° spanning
329 from 1993 to 2018. The Simple Ocean Data Assimilation (SODA) reanalysis version 3.4.2 (40)
330 was used for constructing the depth-dependent velocity profiles. The product is available from
331 1980 to 2018 with a spatial resolution of 0.5° and 50 vertical levels.

332
333 The stratification of the water column was cast by the buoyancy frequency,

$$334 \quad N = \sqrt{\frac{g \partial \rho}{\rho_f \partial z}}, \quad (4)$$

335 where g is the gravitational acceleration, $\frac{\partial \rho}{\partial z}$ is the vertical gradient of the potential density, and ρ_f
336 is the reference density defined above.

337
338 **Contamination Prevention.** To avoid potential contamination, we employed the following
339 protective measures (41): (1) Prior to the cruise, all filters were combusted at 450 °C for >5 h to
340 remove organic matter; (2) Aboard ship, all sample handling was conducted in a laminar flow
341 hood (AirClean 600 Workstation; AirClean Systems), located in a dedicated, clean room with
342 restricted entry where only natural fiber clothing was allowed; vents in this room had AirClean
343 pre-filters taped over them to minimize dust; (3) WTS-LV filter holders were disassembled and
344 soaked in fresh water for 20 minutes, and then thoroughly rinsed with pressurized fresh water, and
345 finally followed by three rinses using 0.2 µm filtered MilliQ water; (4) The clean filter holders
346 were immediately wrapped with pre-combusted foil and stored in the laminar flow hood in the
347 clean room; (5) The laminar flow hood was cleaned and run for at least for 15 min prior to usage
348 and all loading and removal of filters were performed in the laminar flow hood; (6) Tweezers for
349 handling filters were rinsed with 6 nm filtered seawater (from a tangential flow filtration unit)
350 between processing different pore sized filters; and (7) Pre-combusted 47 mm GF/A filters were
351 exposed in the hood during filter loading and sample processing to monitor possible MP
352 contamination. Nitrile gloves and cotton lab coats were worn during field and laboratory work.

353
354 In the laboratory at Harbor Branch Oceanographic Institute: (1) All liquids used for sample
355 processing and analysis (e.g., Milli-Q water, potassium hydroxide solution, ethanol) were filtered
356 through glass-fiber filters prior to use (Whatman GF/F, 0.7 µm pore size, 47 mm diam.); (2) All
357 glass-fiber filters and glassware (e.g., beakers, bowls, scintillation vials, Pasteur pipettes) were
358 covered with aluminum foil, and combusted at 450 °C for >5 h; (3) Steel tweezers were washed

359 with filtered Milli-Q water and flame combusted; (4) All sample preparation was performed in the
360 clean laminar flow under HEPA (high-efficiency particulate air) filtration; (5) Procedural blanks
361 in the lab (n=4) were performed by exposing GF/F filters under the laminar flow when extracting
362 particles from QM-A filters. After the analysis of samples, these four laboratory controls together
363 with four onboard blanks were processed employing the identical procedure as the pump samples.
364 The resultant particles were concentrated on Anodisc filters and scanned by FTIR imaging.

365
366 **Statistical evaluation.** Given that the datasets were not normally distributed (Kolmogorov-
367 Smirnov test), and their variances were not homogeneous (Levene's test), the nonparametric
368 Kruskal-Wallis statistical test was used for multiple comparisons. If the test was significant, pair-
369 wise comparisons were performed using the nonparametric Mann-Whitney-Wilcoxon test. Values
370 of $P < 0.05$ were considered significant. A generalized additive model (GAM) was used to
371 estimate the relationship between the length and the aspect ratio of the identified SMP. All
372 statistical tests and graphs were performed using R software (v.3.4.3, R Development Core Team).

373 374 **Results**

375 **Contamination Controls.** The analysis results of μ FTIR images of procedural blanks showed no
376 positive signals of SMP at Stations B, C and D. One polyurethane particle was confirmed at
377 Station A. In addition, 38 polyacetal particles, determined to originate from WTS-LV pump heads,
378 were identified on 17 out of 48 (35.4%) QM-A filters. The maximum quantity of polyacetal
379 particles detected on a sub-filter was nine, and that was detected at 10 m depth of Station A (*SI*
380 *Appendix*, Table S3). The size of polyacetal MP ranged from 25.6 to 3778.3 μm . The spectra of
381 polyacetal particles are shown in the Fig. S4 (*SI Appendix*). In subsequent data analysis, the
382 number of observed plastics in blanks at each station was subtracted from all datasets of pump
383 samples corresponding to the same station.

384
385 **LMP and SMP Abundance.** In total, 1406 presumptive plastic particles were recovered in the
386 Manta net samples. In a subsample of these particles (n = 457), 452 particles were confirmed as
387 plastics and five could not be classified. The total weight of the Manta net collected particles
388 identified as LMP (n = 452) was 0.619 g, with the averaged LMP mass per particle calculated as
389 0.0014 g. Wind-corrected LMP abundance in the upper 5 m of the SASG varied across the Manta
390 net tow stations, with a range of 0.4-3.0 n m^{-3} (0.6×10^3 - $4.3 \times 10^3 \mu\text{g m}^{-3}$) and an average of 1.5
391 n m^{-3} ($2.1 \times 10^3 \mu\text{g m}^{-3}$). The highest abundance was recorded at Station MT-14 (3.0 n m^{-3} ; $4.3 \times$
392 $10^3 \mu\text{g m}^{-3}$), followed by Stations MT-16 (2.5 n m^{-3} ; $3.5 \times 10^3 \mu\text{g m}^{-3}$), MT-18 (0.8 n m^{-3} ; $1.1 \times$

393 $10^3 \mu\text{g m}^{-3}$), MT-22 (0.7 n m^{-3} ; $0.9 \times 10^3 \mu\text{g m}^{-3}$), with the lowest abundance recorded at Station
394 MT-05 (0.4 n m^{-3} ; $0.6 \times 10^3 \mu\text{g m}^{-3}$). These findings display a general increase in the LMP
395 abundance with proximity to the inner accumulation zone (Fig. 1).

396
397 LMP ($n = 21$) was found in eight out of 15 MultiNet bags at different depths (range 5-60 m, *SI*
398 *Appendix*, Table S1). LMP abundances were from 0 to $1.1 \times 10^{-2} \text{ n m}^{-3}$ ($0\text{-}15.3 \mu\text{g m}^{-3}$) (Fig. 2 A,
399 B, C). Disparities, spanning from 2.4 to over 5 orders of magnitude, were found in the numerical
400 abundances of plastics when comparing SMP from WTS-LV pump to LMP from MultiNet
401 samples in the upper 60 m. After correction of control values and subtraction of all polyacetal
402 polymer signal from our WTS-LV pump samples, SMP particles were detected in 34 of 48
403 analyzed subsamples. A total of 229 particles were confirmed as plastic polymers by μFTIR
404 imaging. The SMP abundance profiles ranged from $0\text{-}244.3 \text{ n m}^{-3}$ and $0\text{-}20.83 \mu\text{g m}^{-3}$ (Fig. 2). No
405 plastics were found at the depth of 3490 m at Station B. SMP abundances were highly variable in
406 our four vertical profiles (Kruskal-Wallis test, $P < 0.05$, *SI Appendix*, Table S4), with the highest
407 mean abundance detected at 10 m at Station A ($218.3 \pm 45.1 \text{ n m}^{-3}$), followed by 60 m at Station
408 D ($85.4 \pm 9.5 \text{ n m}^{-3}$), and 4835 m at Station C ($71.1 \pm 21.5 \text{ n m}^{-3}$) (Fig. 2 A, C, D). Generally,
409 SMP abundances in the vertical profiles decreased with depth, except at Station C (Fig. 2C). In
410 the upper 60 m, the mean abundance of SMP in the outer accumulation zone (Stations A and D,
411 mean: $105.3 \pm 93.9 \text{ n m}^{-3}$, median: 85.4 n m^{-3}) was significantly higher than samples taken from
412 the inner accumulation zone (Stations B and C, mean: $24.4 \pm 24.8 \text{ n m}^{-3}$, median: 17.1 n m^{-3}
413 (Mann-Whitney-Wilcoxon test, $W = 85$, $P = 0.026$, *SI Appendix*, Fig. S5).

414
415 **Polymer Composition.** A total of 12 polymer types, including theoretically buoyant polymers,
416 were identified in the SMP samples (*SI Appendix*, Fig. S6). Five polymer types accounted for
417 more than 80% of the particle count, including polyamide 6/6.6 (PA 6/6.6, 29.3%, $n=67$), alkyd
418 resin (16.2%, $n=37$), PP (15.3%, $n=35$), PE (11.0%, $n=25$) and polyethylene/polypropylene
419 copolymer (PE/PP, 8.7%, $n=20$). The polymer species of each pump sample differed, ranging
420 from 0 to 10 polymer types. PE, PP, PE/PP and Ethylene-ethyl acrylate copolymer (EEA)
421 particles that are lighter than the *in-situ* seawater ($\sim 1.025 \text{ g cm}^{-3}$) were also detected in the
422 ocean's interior (Fig. 3 and *SI Appendix*, Table S5). In the Manta net LMP subsamples, PE was
423 the dominant polymer, corresponding to 79.2% ($n = 358$) of the particles, followed by PP (12.2%,
424 $n = 55$) and PE/PP copolymer (7.3%, $n = 33$). The 1.3% remaining particles ($n = 6$) were
425 identified as PA 6/6.6 ($n = 3$), polyester ($n = 2$) and polystyrene (PS, $n = 1$).

426

427 **Size and Theoretical Sinking Rates of SMP.** The length of SMP particles ranged from 20.1 to
428 321.2 μm (mean = $58.6 \pm 32.4 \mu\text{m}$, median = $49.6 \mu\text{m}$), while the width spanned from 15.9 to
429 126.3 μm (mean = $35.3 \pm 11.6 \mu\text{m}$, median = $35.5 \mu\text{m}$, Fig. S7). A total of 25% ($n = 57$) in the
430 length and 88% ($n = 202$) in the width of all identified plastic particles were less than $40 \mu\text{m}$ long
431 (SS mesh pore size), while 62% (length) and 97% (width) of particles were $<56.6 \mu\text{m}$ (the
432 theoretical diagonal of square SS mesh sieve aperture). The aspect ratio of particles steadily
433 increased with decreases in length (GAM, $R^2 = 0.63$, $P \ll 0.01$, *SI Appendix*, Fig. S8) indicating
434 smaller particles became spherical. The theoretical sinking velocity of SMP particles ($n = 148$)
435 with densities higher than seawater ranged from 2.4×10^{-9} to $1.0 \times 10^{-6} \text{ m s}^{-1}$ (Table S6).

436
437 **Oxidation Degree.** In the Manta net samples, PE-LMP from the outer accumulation zone ($n =$
438 99) of the SASG exhibited modestly higher carbonyl indices in contrast to PE-LMP ($n = 259$)
439 from the inner accumulation zone (Mann-Whitney-Wilcoxon test, $W = 8738$, $P = 1.6 \times 10^{-6}$, Fig.
440 4A). Overall, PE-SMP from WTS-LV pump samples presented significantly higher carbonyl
441 indices than those captured in Manta nets from the identical sampling region within the SASG
442 (Mann-Whitney-Wilcoxon test, the outer accumulation zone, $W = 479$, $P = 9.3 \times 10^{-4}$; the inner
443 accumulation zone, $W = 27$, $P = 1.4 \times 10^{-6}$, Fig. 4A).

444 **Discussion**

446 This study provides the first dataset on the distribution of MP throughout the water column
447 beneath an offshore plastic accumulation zone. Although the dataset is modest and comes from a
448 single expedition, the abundance and composition of MP at different depths from our study
449 provide unique insight into how MP are distributed from the epi- to the abyssopelagic layer within
450 the SASG. Overall, we observed that LMP abundances in net samples (Manta net and MultiNet)
451 were at least two orders of magnitude lower than the SMP abundances concurrently sampled with
452 *in-situ* pumps (Fig. 2, refer to Table S1 for the exact abundance values). These disparities
453 between abundances in the pump and net samples confirm that smaller-sized MP has been largely
454 undercounted and is an important contributor to plastic mass balance in the SASG. Our surface
455 SMP abundances are comparable to existing data ($13\text{-}501 \text{ n m}^{-3}$) from surface waters of the North
456 Atlantic Ocean by Enders et al. (16), who used Raman spectroscopy to identify MP down to 10
457 μm and found over 64% of particles were less than $40 \mu\text{m}$. In comparison to a recent study that
458 employed similar large-volume sampling and automated interpretation μFTIR imaging methods
459 to study the plastic pollution in the deep-water column, SMP abundance ($0\text{-}244.3 \text{ n m}^{-3}$, median:
460 25.6 n m^{-3}) in our study was higher than reported for the Arctic Ocean (size fraction: $25\text{-}50 \mu\text{m}$,

461 abundance: 0-96 n m⁻³, median: 13.0 n m⁻³) (18). It has been shown that smaller-sized MP
462 (typically <150 µm) can translocate into the tissues and organs of organisms upon ingestion,
463 exerting potential negative impacts on marine organisms (19). Investigation of smaller-sized
464 plastics, largely missed in net-based and visual detection-based collections, is pivotal to
465 understanding the ecological impacts of plastic debris as a whole in the ocean ecosystem.

466
467 **Horizontal Distribution.** Floating plastic debris is generally understood to increase in abundance
468 towards the center of oceanic gyres (3-5). In the SASG, Cózar et al. (4) reported differences of a
469 hundred-fold in plastic concentration (>200 µm) between debris within inner and outer
470 accumulation zones, which agree with our Manta net data (Fig. 1). Our observations of lower
471 SMP abundances at water depths <60 m in the inner SASG accumulation zone (Stations B and C)
472 was observed, compared to those in the outer accumulation zone (Stations A and D) (Mann-
473 Whitney-Wilcoxon test, $P < 0.05$, Fig. 2, *SI Appendix*, Fig. S2) are seemingly conflicting with
474 these previous observations. In particular, Station A has the highest abundance of SMP, followed
475 by Stations D, B and C. At present, we are not able to interpret this mismatch with certainty.
476 However, known processes provide a possible explanation for this anomaly. A previous
477 modelling study predicted that 60%-80% of floating debris in the South Atlantic accumulation
478 zone was from South America (42). As the basin-scale circulation largely flows along the isolines
479 of sea surface height, this floating debris from the western border of the South Atlantic would
480 likely arrive first at Station B, followed by Stations A, D and finally Station C (Fig. 5). The
481 floating plastics probably disperses along the proposed route, which may partially contribute to
482 the lower SMP numbers in the near-surface layer of Station C. Additionally, the velocity fields
483 and sea level anomalies on the sampling day of each station (*SI Appendix*, Fig. S9) showed that
484 Stations A and D were closer to the core of the anticyclonic eddies than Stations B and C.
485 Previous model results documented that particles were prone to aggregate at the edges of the
486 anticyclonic eddies (43). Based on a MP field survey in the North Atlantic Gyre, data from
487 satellite observations and models, Brach et al. (44) provided evidence that the anticyclonic eddies
488 could retain, concentrate, and transport MP. High accumulations of near-surface SMP at Stations
489 A and D might also be closely related to these meso- and submesoscale features (Fig. S9). More
490 extensive *in-situ* observations of plastics in the water column will be necessary to resolve the
491 temporal-spatial patterns of water-column MP and verify the possible mechanisms at play.

492
493 **Vertical profiles.** Contrasting profile distribution patterns of MP were observed in the Arctic
494 Ocean among four stations by Tekman et al. (18), who regarded the inconsistent vertical

495 distributions among stations as indications for different mechanisms in the MP flux, highlighting
496 the role of local ocean circulation in the distribution of MP. Similar vertical differences were also
497 observed in our study. SMP abundances at Stations (A, B, D) generally decreased with depth, but
498 contrary to this trend, Station C showed a striking increase of over 20-fold (Fig. 2) at depth. To
499 compare this with the current velocity structure at each station, we computed the climatological
500 depth-dependent velocity profile at the closest grid point of the Simple Ocean Data Assimilation
501 database in 1993-2018 (Fig. 4B). It clearly indicates that the near bottom velocity of bottom
502 currents at Station C was 2-4 times weaker than the other three Stations A, B, and D. We
503 hypothesize that the slower bottom current velocity at Station C was less dilutive and appears to
504 be entraining SMP particles transported to this depth. Although the concurrent presence of both
505 high-abundance SMP and slow currents was only observed at one station, it agrees well with
506 Kane et al. (45) who reported that low intensity currents may accumulate plastic debris in the
507 Tyrrhenian Sea based on a combination of *in-situ* MP measurements and numerical modelling.
508 The accumulation of SMP at depth may also be attributed to the interactions with biological
509 processes (e.g., biofouling, marine aggregate formation and incorporation into fecal pellets),
510 which have been shown to accelerate the downward transport of plastics (46, 47). But the
511 knowledge of water-column MP interactions with biological processes is limited and warrants
512 further research. Additionally, the three-dimensional transportation of plastic particles might
513 contribute to the observed distribution patterns of SMP along the depth continuum (6). Non-
514 metric multidimensional scaling ordination analysis of the polymer composition at each depth
515 supports the clustering of samples into three distinct groups (Fig. 4C, analysis of similarities
516 $R=0.32$, $p=0.005$). In general, high similarity of polymer types between the deep samples and
517 surface samples at different stations (Fig. 4C) was observed, which suggests oceanic SMP
518 particles are dispersed in lateral advection, vertical convection, or a combination of these
519 movements. Further studies of vertical measurements will aid in the understanding of MP
520 transport pathways in the water column.

521
522 Steep density gradients, termed pycnoclines, are known to considerably decelerate settling rates
523 of particles (such as suspended solids, algae or detritus, marine snow, etc.) and prolong their
524 residence times above or within the pycnocline, resulting in a preferential accumulation (48, 49).
525 Recently, several studies have reported higher abundances of MP particles in the pycnocline
526 layers (14, 50, 51). In this study, we deliberately placed high volume pumps within the pycnocline
527 at each station to investigate this phenomenon. At our sampling stations, the maximum buoyancy
528 frequency values (0.021-0.025 s^{-1} , Fig. S10) were larger than 0.016 s^{-1} , indicating that the local

529 stratified layers were well-defined (32). Stratified conditions such as these have been observed
530 entrap marine snow ($\geq 200 \mu\text{m}$) particles (48), yet we only saw a modest peak in pycnocline SMP
531 numbers at one (Station B) of the four sampling stations. It should be noted that Station B
532 displayed the most intense pycnocline conditions from our sample set. However, LMP
533 abundances were observed to increase within pycnocline proximity in the MultiNet samples,
534 particularly MN-01 and -02 (Fig. 2). This difference may reside in the smaller particle size of
535 SMP investigated in this study compared to previous studies (14, 50, 51), whose detectable sizes
536 were limited to MP larger than $100 \mu\text{m}$. The retention time of particles at ocean pycnoclines,
537 increases quadratically with particle size (52), with stratification effects being assessed by
538 comparing the size of settling objects with the fundamental length scale O ($100 \mu\text{m}$ to 1 mm).
539 Thus, objects smaller than $100 \mu\text{m}$ are much less influenced by water stratification (36, 53).
540 Moreover, the theoretically predicted sinking velocities (2.4×10^{-9} to $1.0 \times 10^{-6} \text{ m s}^{-1}$) of SMP
541 particles in our study were at least three orders of magnitude smaller than previously measured
542 settling speeds (1.0×10^{-3} to $250 \times 10^{-3} \text{ m s}^{-1}$) of large MPs ($>300 \mu\text{m}$) and fecal pellets (SI
543 Appendix, Table S6). Notably, SMP size are much smaller than microplastics and fecal pellets of
544 which the settling speeds were previously measured. These extremely low settling velocities of
545 SMP imply higher dispersion, even distribution, and longer lifetime in the water column.
546 Altogether, these factors could explain the lack of retention of SMP particles at isopycnal
547 interfaces. However, the sinking behaviors of SMP may be altered by microbial colonization or
548 incorporation into marine snow and fecal pellets of zooplankton (46, 47). Incorporation of SMP
549 into egested organic materials and marine aggregates, could significantly increase the settling
550 velocity of plastic particles and thus enhance their export from oceanic surface layers and sinking
551 to the seafloor (46), which could result in the reduction of plastic abundances in the upper water
552 column. This undercounting seems especially true with respect to plastics that are denser than the
553 ambient seawater. In contrast, buoyant plastics may be less influenced because these particles can
554 resurface upon aggregate disintegration (54).

555
556 **Chemical Characteristics of Polymer Particles.** The polymer compositions of plastics in WTS-
557 LV pump samples and Manta net samples varied significantly. Overall, PE and PP (91.4%)
558 dominated in the trawl samples, in agreement with findings extensively documented in the
559 literature (4, 5, 7). In contrast, the polymers in the WTS-LV pump samples included PA 6/6.6
560 (29.1%), alkyd resin (16.1%) and polyolefins (PP: 15.2% and PE:10.9%, PE/PP: 8.7%). This
561 incongruity between polymer types collected from pump and Manta net samples verify plastic
562 compositional changes with sampling depth due to size variation, buoyancies and chemical

563 properties of specific polymers. The prevalence of PA in the pelagic water column has also been
564 reported in the Arctic and Pacific Oceans (14, 18). PA is a typical polymer used for fishing nets
565 and ropes. The high number of PA particles indicates that active fisheries in the South Atlantic
566 Ocean (55), may be a sea-based source of PA plastics. Plastic debris sourced from the fishing and
567 other marine activities accounted for over 70% of marine plastic litter by mass on a remote island
568 in the central South Atlantic Ocean (56). Furthermore, polymers with functional groups, like the
569 amide bonds in PA, are susceptible to degradation such as biotransformation and disintegration,
570 relative to more recalcitrant polymers such as PE (57, 58). Enhanced susceptibility to general
571 degradation would accelerate generation of SMP from larger pieces, which could contribute to the
572 higher abundance of smaller PA in the marine environment. The second most abundant polymer
573 type found in our study was alkyd resin. The dominant alkyd resin in marine environments is
574 likely linked to the degradation of the painted surfaces of metal ships (23, 59). As an increasingly
575 busy shipping route from South America to Asia, and a fishing hotspot (55, 60), the South
576 Atlantic Ocean is reasonably susceptible to these paints shedding from commercial and fishery
577 vessels. Ship paints have been shown to disintegrate more rapidly when compared with other
578 plastic polymers and this observation could explain their smaller size distribution in our samples
579 (23, 59).

580
581 The overall inventory from our WTS-LV pumps shows abundant plastic particles smaller than
582 100 μm below the surface of the South Atlantic (*SI Appendix*, Fig. S4). Our pump sampling
583 method was selective for particles that passed through the 40 μm mesh and the size distribution of
584 SMP shows a peak in abundance of fragments around 40 μm (Fig. S4), suggesting the meshes
585 were efficiently selecting for SMP. Meanwhile, SMP abundance peaking around 40 μm also
586 implied that SMP size was not apparently altered by our sample processing steps such as frozen
587 storage at -80°C , water bath sonication treatments and centrifugations. However, several large
588 plastics ($>100 \mu\text{m}$) were observed in the 2-40 μm size fraction. A similar phenomenon was
589 reported in a previous study where a 333 μm neuston net sampling yielded over 60% of non-
590 string-like MP (0.4-1.0 mm) was able to pass through the mesh (61). A possible explanation for
591 the observed size anomaly is the pre-combusted stainless-steel mesh (40 μm) may be deformed
592 under increasing pressure during sampling, allowing larger particles through the mesh. Larger and
593 softer plastic particles could also have worked their way through the 56.6 μm minimal theoretical
594 diagonal of the square SS mesh sieve aperture. Finally, but less likely, the presence of larger
595 plastic particles may also be the result of the overlay or aggregation of small particles during the
596 processing of the samples. For instance, samples were concentrated on the 25 mm Anodisc

597 membrane which was assembled in an open-face 13 mm filter holder, and finally generated an
598 effective filtration area of 133 mm² (~13 mm in diameter) for μ FTIR imaging, which may lead to
599 particles overlaying. It should be mentioned that the boundary geometry of SMP particles
600 measured by this approach suffers from uncertainties, to some extent. The uncertainty in the SMP
601 dimension measurement can be attributed to the low peak-signal-to-noise ratios, which are caused
602 by the irregularities of particle morphology (34), inhomogeneity in chemical composition of
603 plastic materials, or insufficiently removed biofilm (62).

604
605 Manta net collected PE-LMP from the outer accumulation zone had higher carbonyl indices than
606 from the inner accumulation zone (Fig. 4A) suggesting a longer residence time for these LMP.
607 However, this finding is in disagreement with previous research (63, 64), that reported plastic
608 particles displaying a higher degree of oxidation offshore along a transect. A possible explanation
609 for this discrepancy is that the literature datasets were from the inshore to offshore samples, in
610 contrast to all samples from the SASG in our study, where plastic particles with different
611 oxidative history were entrapped and move with the flow in the gyre. Therefore, it is plausible
612 that PE-LMP retained in the gyre for a longer time was coincidentally captured in the outer
613 accumulation zone. Higher carbonyl indices were observed for SMP collected by WTS-LV
614 pumps compared to LMP collected with Manta nets, suggesting SMP were potentially more
615 degraded than LMP. A similar result was obtained by Ter Halle et al. (65), who found a
616 significant decrease in the molar mass from mesoplastic to MP sampled from the North Atlantic
617 Gyre, which suggests that small plastics are more oxidized than larger ones. These data also agree
618 with previous findings for the model of plastic degradation, which denotes that plastic degrades
619 into smaller fragments and these daughter fragments are likely to be more oxidized than parent
620 fragments due to their different chemical and physical properties (2). It should be noted that
621 specific polymer types exhibit variation in carbonyl indices, which underlines the need for a
622 larger database and development of other reliable methods to evaluate the weathering degree of
623 plastics in the environment.

624
625 The appreciable amounts of SMP in the ocean's interior unveiled here suggest a potential
626 ecosystem-wide impact. Compared to LMP, SMP are more readily ingested by marine particle
627 feeders because of their small size and the smaller-sized plastic has the ability to translocate to
628 internal tissues in organisms (66), resulting in bioaccumulation of MP and its associated
629 chemicals at multiple trophic levels (67). Methods for the quantification of water-column SMP in
630 the open ocean is new and results are therefore relatively uncommon, however, the current study

631 together with two previous studies all revealed unexpectedly high numbers of SMP in the ocean's
632 interior and varied with depth (18, 22). Previous reports have estimated mean MP abundances in
633 the upper 200 m of an Atlantic North-South transect as high as 2272 n m⁻³ (22). Based on all these
634 depth-resolved observations, it is reasonable to consider the following scenario: large amounts of
635 SMP accumulate at certain depths, forming a high plastic-to-marine biota ratio, thus increasing
636 the probability of encountering and ingesting plastic particles by marine organisms (14, 68). For
637 instance, comparing our measured SMP abundances (0-244.3 n m⁻³) to previously measured total
638 copepod abundance (0-12 n m⁻³) at depth of 0-3000 m (69) in the South Atlantic, it is plausible
639 that copepods would encounter these abundant plastics at certain depths. Furthermore, the impacts
640 of SMP on marine fauna could be exacerbated by the combination of more aged surface
641 properties and large-aspect ratios (*SI Appendix*, Fig. S5), both of which have been experimentally
642 documented to enhance MP ingestion (47, 70). Field evidence showed that MP (40-200 μm)
643 constituted roughly 26% of all plastic particles ingested by mesopelagic fishes in the northwest
644 Atlantic Ocean (71), and 45% of deep-sea benthic amphipods in the North East Atlantic contained
645 translocated MP in soft tissues, of which PA was the dominant polymer type consistently found
646 (72). As commercial fishing efforts scale up to harvest marine species for human consumption,
647 studies focusing on smaller MP ingestion are urgently needed to assess the extent of plastic
648 contamination in biomass, which may represent a large fraction of the 'missing' plastics (73).
649 Marine organisms grazing on MP also have potential impacts on global biogeochemical cycling.
650 Employing an Earth system model, Kvale et al (74) predicted that zooplankton ingesting
651 microplastics could accelerate global deoxygenation by an extra 0.2-0.5% relative to 1960 values
652 by the year 2020 and reduce the oxygen inventory in the North Pacific by up to 10%.

653
654 Our results show that highly abundant SMP dominate surface to near-seafloor waters in the
655 plastic accumulation zone of the South Atlantic and form microplastic hotspots at certain depths,
656 implicating the ocean interior as a crucial pool of 'missing' plastics, particularly in low-flow
657 regimes. The abundances and distributions patterns of SMP varied geographically and vertically
658 due to the diverse and complex redistribution processes interacting with different plastic particles.
659 Compared with net-collected LMP, SMP particles are more highly oxidized and appear to have a
660 longer lifetime in the water column, suggesting increased marine ecosystem health risks through
661 possible bio-uptake of plastic particles and associated chemicals (75) and potential impacts to
662 global biogeochemical cycles (74). SMP are distinguished from LMP with respect to their high
663 abundance, chemical nature, transport behavior, weathering stages, interactions with ambient
664 environments, bioavailability and the release efficiency of plastic additives (57). These distinct

665 characteristics impact their environmental fate and potential impacts on marine ecosystems.
666 Given the fundamental elements of our findings, this study of the SASG strongly suggests that
667 SMP, largely unaccounted in previous studies, is a critical and unique component in ocean plastic
668 inventories. Additionally, our study provides a stimulus for additional work to interpret and
669 understand the fate and potential impacts of microplastics in aquatic systems in general.

670 **Acknowledgments:** The authors thank the crew and scientists aboard the NIOZ RV *Pelagia*
671 cruise 64PE448. This work was supported by start-up funds from NIOZ to L.A. A.-Z. to help fund
672 the expedition. Funds for this study came from: FAU World Class Faculty and Scholar Program
673 to TJM; a NOAA marine debris grant NA17NOS9990024 awarded to L.A.A.-Z. and T.J.M., and
674 the American Chemistry Council awarded to L.A.A.-Z., E.Z, and T.J.M.

675 **Author Contributions:** S.Z., E.R.Z, L.A.A-Z., and T.J.M. designed research; S.Z., E.R.Z.,
676 R.P.B., and L.A.A.-Z performed research; S.Z., E.R.Z., R.P.B., P.L., and T.J.M. analyzed data;
677 S.Z. wrote the first draft of the paper, all coauthors were involved in editing subsequent versions.
678 Competing Interest Statement: The authors declare no competing interest.

679 **Data and materials availability:** All data needed to evaluate the conclusions in the paper are
680 present in the paper and/or the Supplementary Materials. Additional data related to this paper may
681 be requested from the authors.

682 683 **References**

- 684 1. S. B. Borrelle *et al.*, Predicted growth in plastic waste exceeds efforts to mitigate plastic
685 pollution. *Science* **369**, 1515-1518 (2020). <https://doi.org/10.1126/science.aba3656>
- 686 2. A. L. Andrady, The plastic in microplastics: A review. *Marine pollution bulletin* **119**, 12-
687 22 (2017). <https://doi.org/10.1016/j.marpolbul.2017.01.082>
- 688 3. E. Van Sebille *et al.*, A global inventory of small floating plastic debris. *Environmental*
689 *Research Letters* **10**, 124006 (2015). <https://doi.org/10.1088/1748-9326/10/12/124006>
- 690 4. A. Cózar *et al.*, Plastic debris in the open ocean. *Proceedings of the National Academy of*
691 *Sciences* **111**, 10239-10244 (2014). <https://doi.org/10.1073/pnas.1314705111>
- 692 5. M. Eriksen *et al.*, Plastic pollution in the world's oceans: more than 5 trillion plastic pieces
693 weighing over 250,000 tons afloat at sea. *PloS One* **9**, e111913 (2014).
694 <https://doi.org/10.1371/journal.pone.0111913>
- 695 6. E. Van Sebille *et al.*, The physical oceanography of the transport of floating marine debris.
696 *Environmental Research Letters* **15**, 023003 (2020). [https://doi.org/10.1088/1748-
697 9326/ab6d7d](https://doi.org/10.1088/1748-9326/ab6d7d)

- 698 7. K. L. Law *et al.*, Plastic accumulation in the North Atlantic subtropical gyre. *Science* **329**,
699 1185-1188 (2010). <https://doi.org/10.1126/science.1192321>
- 700 8. M. Bergmann, M. B. Tekman, L. Gutow, Marine litter: Sea change for plastic pollution.
701 *Nature* **544**, 297 (2017). <https://doi.org/10.1038/544297a>
- 702 9. L. C. Woodall *et al.*, The deep sea is a major sink for microplastic debris. *Royal Society*
703 *Open Science* **1**, 140317 (2014). <https://doi.org/10.1098/rsos.140317>
- 704 10. F. Pohl, J. T. Eggenhuisen, I. A. Kane, M. A. Clare, Transport and burial of microplastics
705 in deep-marine sediments by turbidity currents. *Environmental Science & Technology* **54**,
706 4180-4189 (2020). <https://doi.org/10.1021/acs.est.9b07527>
- 707 11. B. H. Robison, Conservation of deep pelagic biodiversity. *Conservation Biology* **23**, 847-
708 858 (2009). <https://doi.org/10.1111/j.1523-1739.2009.01219.x>
- 709 12. L. A. Levin *et al.*, Global observing needs in the deep ocean. *Frontiers in Marine Science*
710 **6**, 241 (2019). <https://doi.org/10.3389/fmars.2019.00241>
- 711 13. K. K. La Daana *et al.*, Microplastics in sub-surface waters of the Arctic Central Basin.
712 *Marine Pollution Bulletin* **130**, 8-18 (2018).
713 <https://doi.org/10.1016/j.marpolbul.2018.03.011>
- 714 14. C. A. Choy *et al.*, The vertical distribution and biological transport of marine
715 microplastics across the epipelagic and mesopelagic water column. *Scientific Reports* **9**,
716 7843 (2019). <https://doi.org/10.1038/s41598-019-44117-2>
- 717 15. P. S. Ross *et al.*, Pervasive distribution of polyester fibres in the Arctic Ocean is driven by
718 Atlantic inputs. *Nature Communications* **12**, 106 (2021). <https://doi.org/10.1038/s41467-020-20347-1>
- 719
- 720 16. K. Enders, R. Lenz, C. A. Stedmon, T. G. Nielsen, Abundance, size and polymer
721 composition of marine microplastics $\geq 10 \mu\text{m}$ in the Atlantic Ocean and their modelled
722 vertical distribution. *Marine Pollution Bulletin* **100**, 70-81 (2015).
723 <https://doi.org/10.1016/j.marpolbul.2015.09.027>
- 724 17. C. Lorenz *et al.*, Spatial distribution of microplastics in sediments and surface waters of
725 the southern North Sea. *Environmental Pollution* **252**, 1719-1729 (2019).
726 <https://doi.org/10.1016/j.envpol.2019.06.093>
- 727 18. M. B. Tekman *et al.*, Tying up loose ends of microplastic pollution in the Arctic:
728 Distribution from the sea surface, through the water column to deep-sea sediments at the
729 HAUSGARTEN observatory. *Environmental Science & Technology*, **54**, 4079-4090
730 (2020). <https://doi.org/10.1021/acs.est.9b06981>

- 731 19. A. Lusher, P. Hollman, J. Mendoza-Hill, "Microplastics in fisheries and aquaculture:
732 status of knowledge on their occurrence and implications for aquatic organisms and food
733 safety" (FAO Fisheries and Aquaculture Technical Paper No. 615. Rome, Italy, 2017).
- 734 20. GESAMP, "Sources, fate and effects of microplastics in the marine environment: part two
735 of a global assessment" (GESAMP No. 93, International Maritime Organization, London,
736 2016).
- 737 21. A. Ter Halle *et al.*, Nanoplastic in the North Atlantic subtropical gyre. *Environmental
738 Science & Technology* **51**, 13689-13697 (2017). <https://doi.org/10.1021/acs.est.7b03667>
- 739 22. K. Pabortsava, R. S. Lampitt, High concentrations of plastic hidden beneath the surface of
740 the Atlantic Ocean. *Nature Communications* **11**, 4073 (2020).
741 <https://doi.org/10.1038/s41467-020-17932-9>
- 742 23. A. L. d. F. Lacerda *et al.*, Plastics in sea surface waters around the Antarctic Peninsula.
743 *Scientific Reports* **9**, 1-12 (2019). <https://doi.org/10.1038/s41598-019-40311-4>
- 744 24. J. K. Bishop, P. J. Lam, T. J. Wood, Getting good particles: Accurate sampling of particles
745 by large volume in-situ filtration. *Limnology and Oceanography: Methods* **10**, 681-710
746 (2012). <https://doi.org/10.4319/lom.2012.10.681>
- 747 25. S. Primpke, M. Wirth, C. Lorenz, G. Gerdt, Reference database design for the automated
748 analysis of microplastic samples based on Fourier transform infrared (FTIR) spectroscopy.
749 *Analytical and Bioanalytical Chemistry* **410**, 5131-5141 (2018).
750 <https://doi.org/10.1007/s00216-018-1156-x>
- 751 26. J. A. Brandon, A. Freibott, L. M. Sala, Patterns of suspended and salp-ingested
752 microplastic debris in the North Pacific investigated with epifluorescence microscopy.
753 *Limnology and Oceanography Letters* **5**, 46-53 (2020). <https://doi.org/10.1002/lo12.10127>
- 754 27. J. A. Brandon, M. Goldstein, M. D. Ohman, Long-term aging and degradation of
755 microplastic particles: Comparing in situ oceanic and experimental weathering patterns.
756 *Marine Pollution Bulletin* **110**, 299-308 (2016).
757 <https://doi.org/10.1016/j.marpolbul.2016.06.048>
- 758 28. L. Canopoli, F. Coulon, S. T. Wagland, Degradation of excavated polyethylene and
759 polypropylene waste from landfill. *Science of the Total Environment* **698**, 134125 (2020).
- 760 29. A. Moldovan, R. Buican, S. Patachia, M. Tiorean, Characterization of polyolefins wastes
761 by FTIR spectroscopy. *Bulletin of the Transilvania University of Brasov. Engineering
762 Sciences. Series I* **5**, 65 (2012). <https://doi.org/10.1016/j.scitotenv.2019.134125>

- 763 30. A. Mendoza, G. Kortaberria, F. F. Marzo, U. Mayor, O. C. Basurko, C. Peña-Rodriguez,
764 Solvent-Based Elimination of Organic Matter from Marine-Collected Plastics,
765 *Environments* **8**, 68 (2021). <https://doi.org/10.3390/environments8070068>
- 766 31. A. I. Catarino, V. Macchia, W. G. Sanderson, R. C. Thompson, T. B. Henry, Low levels of
767 microplastics (MP) in wild mussels indicate that MP ingestion by humans is minimal
768 compared to exposure via household fibres fallout during a meal, *Environmental Pollution*
769 **237**, 675-684 (2018). <https://doi.org/10.1016/j.envpol.2018.02.069>
- 770 32. J. C. Prata *et al.*, Preparation of biological samples for microplastic identification by Nile
771 Red. *Science of The Total Environment* **783**, 147065 (2021).
772 <https://doi.org/10.1016/j.scitotenv.2021.147065>
- 773 33. M. Simon, N. van Alst, J. Vollertsen, Quantification of microplastic mass and removal
774 rates at wastewater treatment plants applying Focal Plane Array (FPA)-based Fourier
775 Transform Infrared (FT-IR) imaging. *Water Research* **142**, 1-9 (2018).
776 <https://doi.org/10.1016/j.watres.2018.05.019>
- 777 34. M. G. J. Löder, M. Kuczera, S. Mintenig, C. Lorenz, G. Gerdt, Focal plane array
778 detector-based micro-Fourier-transform infrared imaging for the analysis of microplastics
779 in environmental samples. *Environmental Chemistry* **12**, 563-581 (2015).
780 <https://doi.org/10.1071/EN14205>
- 781 35. R. G. Kumar, K. B. Strom, A. Keyvani, Floc properties and settling velocity of San
782 Jacinto estuary mud under variable shear and salinity conditions. *Continental Shelf*
783 *Research* **30**, 2067-2081 (2010). <https://doi.org/10.1016/j.csr.2010.10.006>
- 784 36. A. Ardekani, R. Stocker, Stratlets: low Reynolds number point-force solutions in a
785 stratified fluid. *Physical Review Letters* **105**, 084502 (2010).
786 <https://doi.org/10.1103/PhysRevLett.105.084502>
- 787 37. T. Kukulka, G. Proskurowski, S. Morét-Ferguson, D. Meyer, K. Law, The effect of wind
788 mixing on the vertical distribution of buoyant plastic debris. *Geophysical Research Letters*
789 **39**, (2012). <https://doi.org/10.1029/2012GL051116>
- 790 38. M. Egger, F. Sulu-Gambari, L. Lebreton, First evidence of plastic fallout from the North
791 Pacific Garbage Patch. *Scientific Reports* **10**, 7495 (2020). <https://doi.org/10.1038/s41598-020-64465-8>
- 792
793 39. J. Reisser *et al.*, The vertical distribution of buoyant plastics at sea: an observational study
794 in the North Atlantic Gyre. *Biogeosciences* **12**, 1249-1256 (2015).
795 <https://doi.org/10.5194/bg-12-1249-2015>

- 796 40. J. A. Carton, G. A. Chepurin, L. Chen, SODA3: A new ocean climate reanalysis. *Journal*
797 *of Climate* **31**, 6967-6983 (2018). <https://doi.org/10.1175/JCLI-D-18-0149.1>
- 798 41. S. Zhao, M. Danley, J. E. Ward, D. Li, T. J. Mincer, An approach for extraction,
799 characterization and quantitation of microplastic in natural marine snow using Raman
800 microscopy. *Analytical Methods* **9**, 1470-1478 (2017).
801 <https://doi.org/10.1039/C6AY02302A>
- 802 42. L.-M. Lebreton, S. Greer, J. C. Borrero, Numerical modelling of floating debris in the
803 world's oceans. *Marine Pollution Bulletin* **64**, 653-661 (2012).
804 <https://doi.org/10.1016/j.marpolbul.2011.10.027>
- 805 43. A. Samuelsen, S. S. Hjøllo, J. A. Johannessen, R. Patel, Particle aggregation at the edges
806 of anticyclonic eddies and implications for distribution of biomass. *Ocean Science* **8**, 389-
807 400 (2012). <https://doi.org/10.5194/os-8-389-2012>
- 808 44. L. Brach *et al.*, Anticyclonic eddies increase accumulation of microplastic in the North
809 Atlantic subtropical gyre. *Marine Pollution Bulletin* **126**, 191-196 (2018).
810 <https://doi.org/10.1016/j.marpolbul.2017.10.077>
- 811 45. I. A. Kane *et al.*, Seafloor microplastic hotspots controlled by deep-sea circulation.
812 *Science* **368**, 1140-1145 (2020). <https://doi.org/10.1126/science.aba5899>
- 813 46. L. A. Amaral-Zettler, E. R. Zettler, T. J. Mincer, M. A. Klaassen, S. M. Gallager,
814 Biofouling impacts on polyethylene density and sinking in coastal waters: A macro/micro
815 tipping point? *Water Research*, 117289 (2021).
816 <https://doi.org/10.1016/j.watres.2021.117289>
- 817 47. S. Zhao, J. E. Ward, M. Danley, T. J. Mincer, Field-based evidence for microplastic in
818 marine aggregates and mussels: implications for trophic transfer. *Environmental Science*
819 *& Technology* **52**, 11038-11048 (2018). <https://doi.org/10.1021/acs.est.8b03467>
- 820 48. S. MacIntyre, A. L. Alldredge, C. C. Gotschalk, Accumulation of marines now at density
821 discontinuities in the water column. *Limnology and Oceanography* **40**, 449-468 (1995).
822 <https://doi.org/10.4319/lo.1995.40.3.0449>
- 823 49. M. M. Mrokowska, Influence of pycnocline on settling behaviour of non-spherical particle
824 and wake evolution. *Scientific Reports* **10**, 20595 (2020). <https://doi.org/10.1038/s41598-020-77682-y>
- 825
826 50. M. Zobkov, E. Esiukova, A. Zyubin, I. Samusev, Microplastic content variation in water
827 column: The observations employing a novel sampling tool in stratified Baltic Sea.
828 *Marine Pollution Bulletin* **138**, 193-205 (2019).
829 <https://doi.org/10.1016/j.marpolbul.2018.11.047>

- 830 51. E. Uurasjärvi, M. Pääkkönen, O. Setälä, A. Koistinen, M. Lehtiniemi, Microplastics
831 accumulate to thin layers in the stratified Baltic Sea. *Environmental Pollution* **268**, 115700
832 (2021). <https://doi.org/10.1016/j.envpol.2020.115700>
- 833 52. K. Kindler, A. Khalili, R. Stocker, Diffusion-limited retention of porous particles at
834 density interfaces. *Proceedings of the National Academy of Sciences* **107**, 22163-22168
835 (2010). <https://doi.org/10.1073/pnas.1012319108>
- 836 53. A. Doostmohammadi, R. Stocker, A. M. Ardekani, Low-Reynolds-number swimming at
837 pycnoclines. *Proceedings of the National Academy of Sciences* **109**, 3856-3861 (2012).
838 <https://doi.org/10.1073/pnas.1116210109>
- 839 54. M. Kooi, E. H. van Nuns, M. Scheffer, A. A. Koelmans, Ups and downs in the ocean:
840 Effects of biofouling on vertical transport of microplastics. *Environmental Science &*
841 *Technology* **51**, 7963-7971 (2017). <https://doi.org/10.1021/acs.est.6b04702>
- 842 55. T. A. Clay *et al.*, A comprehensive large-scale assessment of fisheries bycatch risk to
843 threatened seabird populations. *Journal of Applied Ecology* **56**, 1882-1893 (2019).
844 <https://doi.org/10.1111/1365-2664.13407>
- 845 56. P. G. Ryan, The transport and fate of marine plastics in South Africa and adjacent oceans.
846 *South African Journal of Science* **116**, 1-9 (2020).
847 <http://dx.doi.org/10.17159/sajs.2020/7677>
- 848 57. B. Gewert, M. M. Plassmann, M. MacLeod, Pathways for degradation of plastic polymers
849 floating in the marine environment. *Environmental Science: Processes & Impacts* **17**,
850 1513-1521 (2015). <http://dx.doi.org/10.1039/C5EM00207A>
- 851 58. K. Min, J. D. Cuiffi, R. T. Mathers, Ranking environmental degradation trends of plastic
852 marine debris based on physical properties and molecular structure. *Nature*
853 *Communications* **11**, 727 (2020). <https://doi.org/10.1038/s41467-020-14538-z>
- 854 59. Y. K. Song, S. H. Hong, M. Jang, G. M. Han, W. J. Shim, Occurrence and distribution of
855 microplastics in the sea surface microlayer in Jinhae Bay, South Korea. *Archives of*
856 *Environmental Contamination and Toxicology* **69**, 279-287 (2015).
857 <https://doi.org/10.1007/s00244-015-0209-9>
- 858 60. P. G. Ryan, B. J. Dilley, R. A. Ronconi, M. Connan, Rapid increase in Asian bottles in the
859 South Atlantic Ocean indicates major debris inputs from ships. *Proceedings of the*
860 *National Academy of Sciences* **116**, 20892-20897 (2019).
861 <https://doi.org/10.1073/pnas.1909816116>

- 862 61. T. Tokai, K. Uchida, M. Kuroda, A. Isobe, Mesh selectivity of neuston nets for
863 microplastics. *Marine Pollution Bulletin* **165**, 112111 (2021).
864 <https://doi.org/10.1016/j.marpolbul.2021.112111>
- 865 62. J. P. Harrison, M. Schratzberger, M. Sapp, A. M. Osborn, Rapid bacterial colonization of
866 low-density polyethylene microplastics in coastal sediment microcosms. *BMC*
867 *Microbiology* **14**, 232 (2014). <https://doi.org/10.1186/s12866-014-0232-4>
- 868 63. E. Martí *et al.*, The Colors of the Ocean Plastics. *Environmental Science & Technology* **54**,
869 6594-6601 (2020). <https://doi.org/10.1021/acs.est.9b06400>
- 870 64. J. Brandon, M. Goldstein, M. D. Ohman, Long-term aging and degradation of microplastic
871 particles: comparing in situ oceanic and experimental weathering patterns. *Marine*
872 *Pollution Bulletin* **110**, 299-308 (2016). <https://doi.org/10.1016/j.marpolbul.2016.06.048>
- 873 65. A. Ter Halle *et al.*, To what extent are microplastics from the open ocean weathered?
874 *Environmental Pollution* **227**, 167-174 (2017).
875 <https://doi.org/10.1016/j.envpol.2017.04.051>
- 876 66. H. K. Mcllwraith, J. Kim, P. Helm, S. P. Bhavsar, J. S. Metzger, and C. M. Rochman,
877 Evidence of Microplastic Translocation in Wild-Caught Fish and Implications for
878 Microplastic Accumulation Dynamics in Food Webs. *Environmental Science &*
879 *Technology* **55**, 12372-12382 (2021). <https://doi.org/10.1021/acs.est.1c02922>
- 880 67. M. E. Miller, M. Hamann, F. J. Kroon, Bioaccumulation and biomagnification of
881 microplastics in marine organisms: A review and meta-analysis of current data. *Plos One*
882 **15**, eo240792 (2020). <https://doi.org/10.1371/journal.pone.0240792>
- 883 68. J. M. Gove *et al.*, Prey-size plastics are invading larval fish nurseries. *Proceedings of the*
884 *National Academy of Sciences* **116**, 24143-24149 (2019).
885 <https://doi.org/10.1073/pnas.1907496116>
- 886 69. A. Vereshchaka, G. Abyzova, A. Lunina, E. Musaeva, The deep-sea zooplankton of the
887 North, Central, and South Atlantic: biomass, abundance, diversity. *Deep Sea Research*
888 *Part II: Topical Studies in Oceanography* **137**, 89-101 (2017).
889 <https://doi.org/10.1016/j.dsr2.2016.06.017>
- 890 70. R. J. Vroom, A. A. Koelmans, E. Besseling, C. Halsband, Aging of microplastics
891 promotes their ingestion by marine zooplankton. *Environmental Pollution* **231**, 987-996
892 (2017). <https://doi.org/10.1016/j.envpol.2017.08.088>
- 893 71. A. M. Wieczorek *et al.*, Frequency of microplastics in mesopelagic fishes from the
894 Northwest Atlantic. *Frontiers in Marine Science* **5**, 39 (2018).
895 <https://doi.org/10.3389/fmars.2018.00039>

- 896 72. W. Courtene-Jones, B. Quinn, C. Ewins, S. F. Gary, B. E. Narayanaswamy, Consistent
897 microplastic ingestion by deep-sea invertebrates over the last four decades (1976–2015), a
898 study from the North East Atlantic. *Environmental Pollution* **244**, 503-512 (2019).
899 <https://doi.org/10.1016/j.envpol.2018.10.090>
- 900 73. K. Kvale, A. Prowe, C.-T. Chien, A. Landolfi, A. Oschlies, The global biological
901 microplastic particle sink. *Scientific Reports* **10**, 16670 (2020).
902 <https://doi.org/10.1038/s41598-020-72898-4>
- 903 74. K. Kvale, A. Prowe, C.-T. Chien, A. Landolfi, A. Oschlies, Zooplankton grazing of
904 microplastic can accelerate global loss of ocean oxygen. *Nature Communications* **12**,
905 2358 (2021). <https://doi.org/10.1038/s41467-021-22554-w>
- 906 75. M. MacLeod, H. P. H. Arp, M. B. Tekman, A. Jahnke, The global threat from plastic
907 pollution. *Science* **373**, 61-65 (2021). <https://doi.org/10.1126/science.abg5433>
- 908
909
910
911
912
913
914

915 Figure legends

916 **Fig. 1. Map of the Manta net, MultiNet, and WTS-LV pumps sampling locations.** Blue
917 triangles represent four WTS-LV pump sampling stations (A, B, C, D). Green shaded bubbles
918 indicate the five Manta net tow stations (MT-05, -14, -16, -18, -22) and size of circles reflects the
919 wind-corrected LMP (0.3-5.0 mm) abundances. Red diamonds represent the three Multinet
920 sampling stations (MN-01, -02, and 03). Surface LMP abundances ($n\ m^{-3}$) in the South Atlantic
921 Ocean by Eriksen et al. (5) are contoured using the Kriging interpolation method based on the
922 surface-trawl datasets (gray dots). The blue arrows represent the schematic circulation in the
923 South Atlantic.

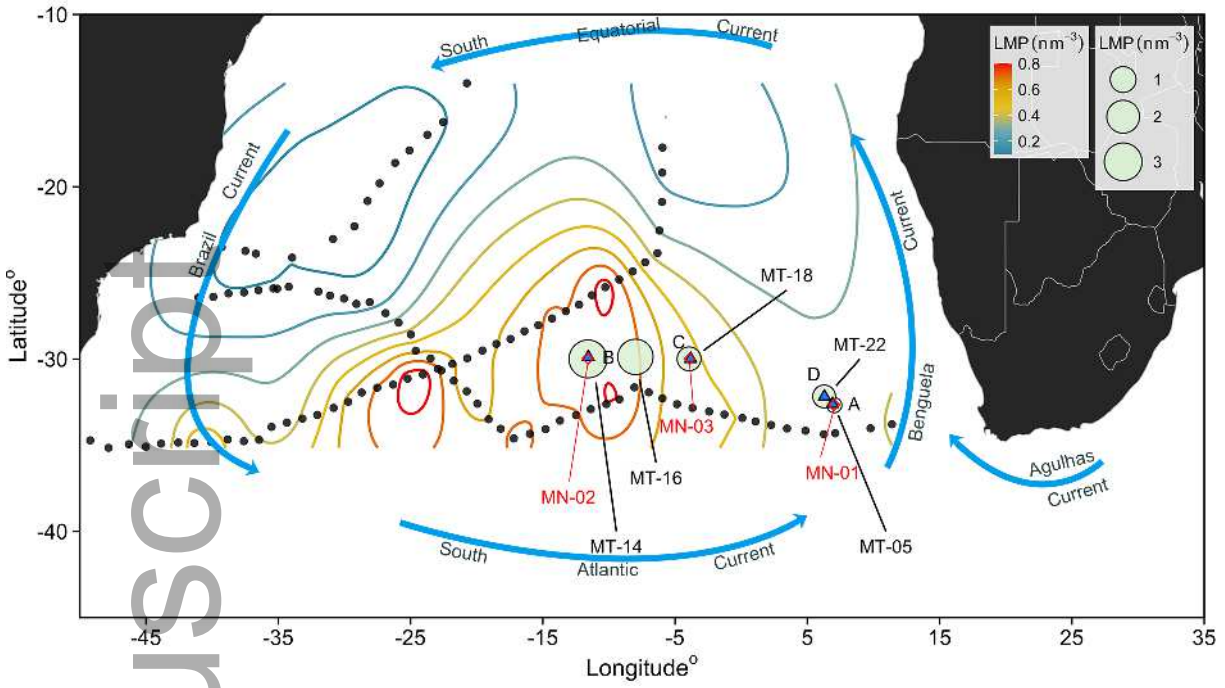
924 **Fig. 2. Numerical, mass abundances of MP collected with the Manta net, MultiNet, and**
925 **WTS-LV pump.** (A) Station A, (B) Station B, (C) Station C, (D) Station D. The filled colors of
926 points correspond to the respective x-axis. The values of the Manta net sample have been
927 corrected for wind-induced mixing in the 5-m-thick ocean layer. The numerical abundances of
928 plastics in the Manta net and MultiNet samples were log transformed. Yellow triangles represent
929 the MultiNet samples in which no plastic fragments were found. Gray and light blue shades

930 indicate the top 5 m of water column and approximate pycnocline layer, respectively. Error bars
931 represent standard deviation.

932 **Fig. 3. Polymer composition profiles of SMP collected with WTS-LV pumps at four stations.**
933 (A) Station A, (B) Station B, (C) Station C, (D) Station D.

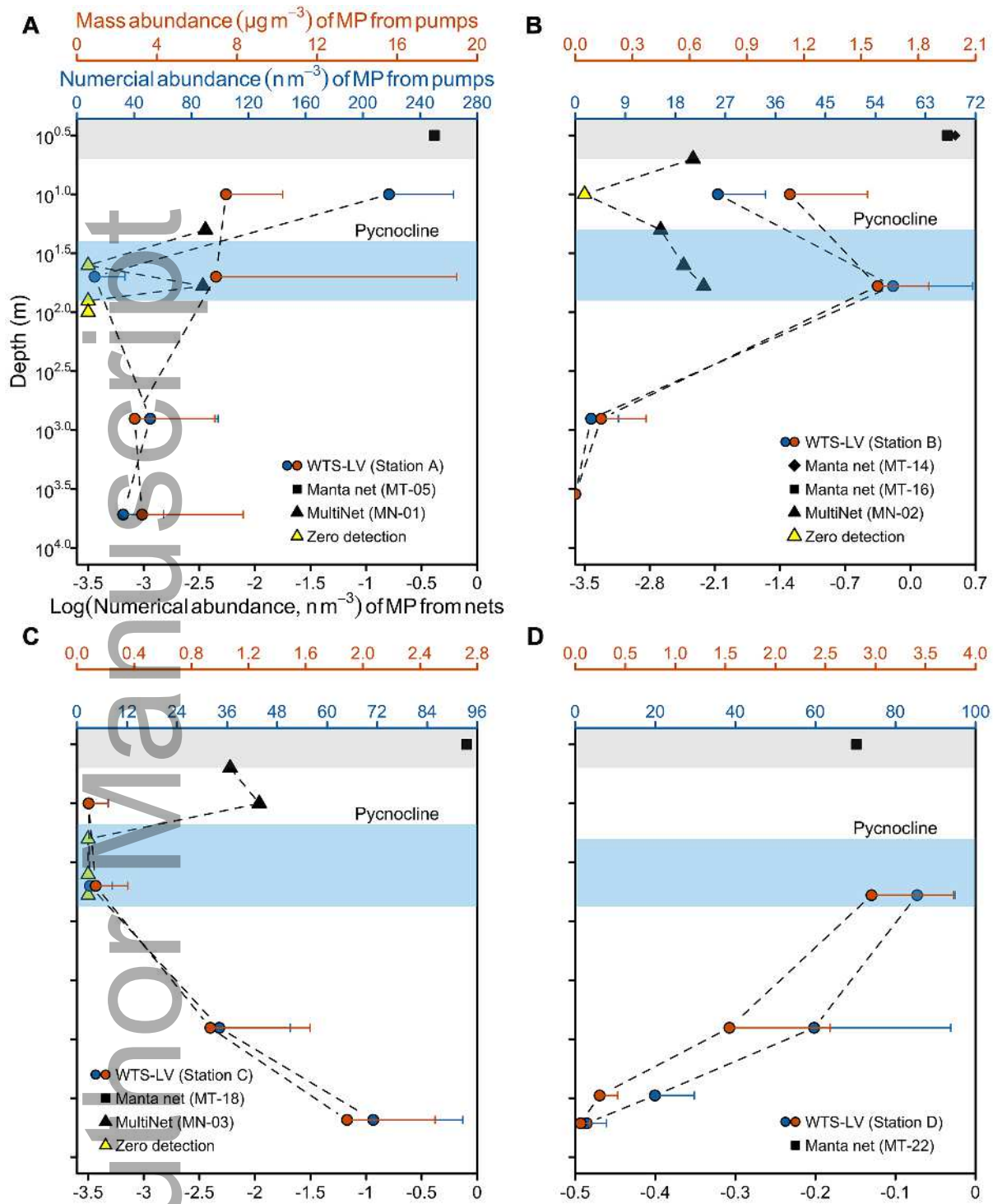
934
935
936
937
938
939
940 **Fig. 4. (A)** Carbonyl indices of polyethylene particles from the Manta net (orange boxplots) and
941 WTS-LV pump (yellow boxplots) in the SASG. The “Outer” and “Inner” indicate the sampling
942 regions located in the outer and inner accumulation zones of the SASG as shown in Fig. 1. Bold
943 black horizontal lines represent boxplot medians; top and bottom of colored boxes represent 25th
944 and 75th percentiles; and whiskers indicate the largest and the smallest measured values within
945 1.5 interquartile ranges from the box. Asterisks denote statistically significant differences between
946 LMP and SMP (Mann-Whitney-Wilcoxon test, $p < 0.05$). (B) The depth-dependent velocity
947 profiles ($\text{m s}^{-1} \times 10^{-2}$) at the four sampling stations averaged over 1993-2018. The dataset is from
948 the Simple Ocean Data Assimilation reanalysis. (C) Non-metric multidimensional scaling (NMDS)
949 ordination of polymer type composition identified in WTS-LV samples at each depth from all
950 stations based on Bray-Curtis dissimilarities (Stress = 0.11). Ellipses in NMDS denote 95%
951 confidence levels for the distinct clustering. Colored shapes represent four WTS-LV pump
952 stations. The text labels indicate the sampling depth.

953
954 **Fig. 5. Surface circulation in the South Atlantic.** The mean sea surface height (m, color) with
955 surface geostrophic velocities overlaid (m s^{-1} , vectors) over the South Atlantic during 1993-2018.
956 The sampling locations are marked as red triangles. The dataset was obtained from the CMEMS.

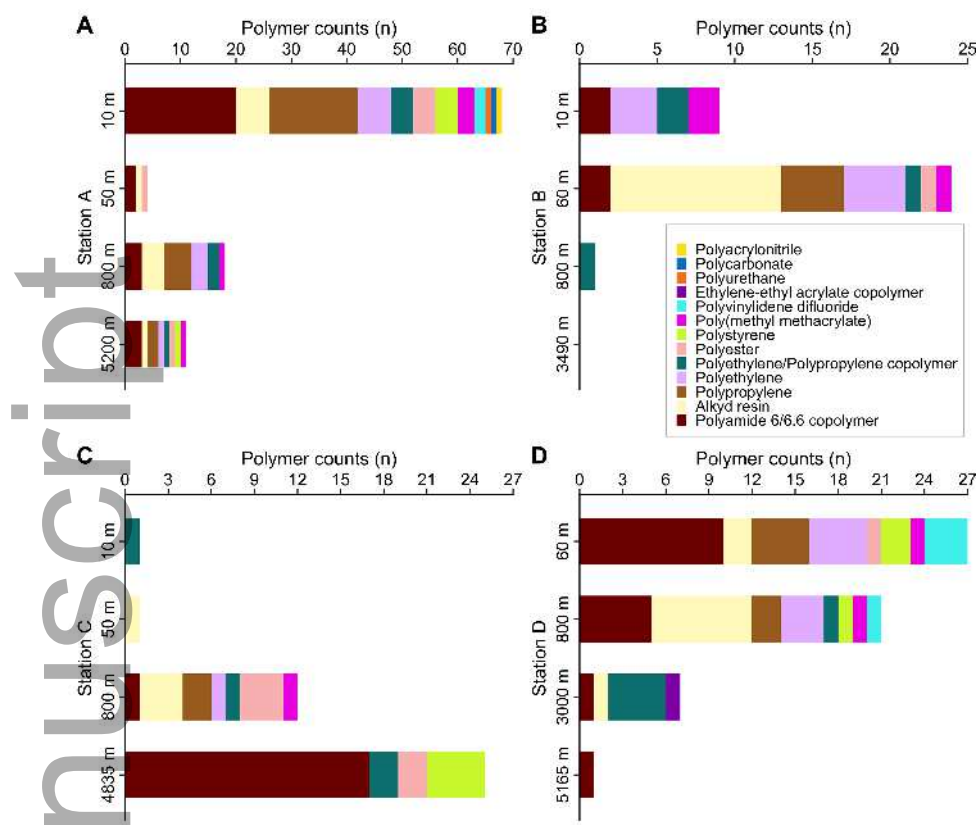


gcb_16089_f1.tif

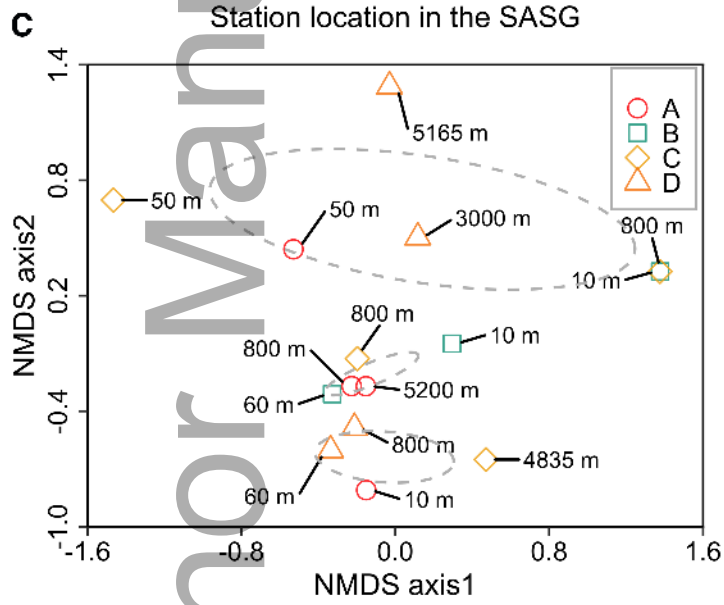
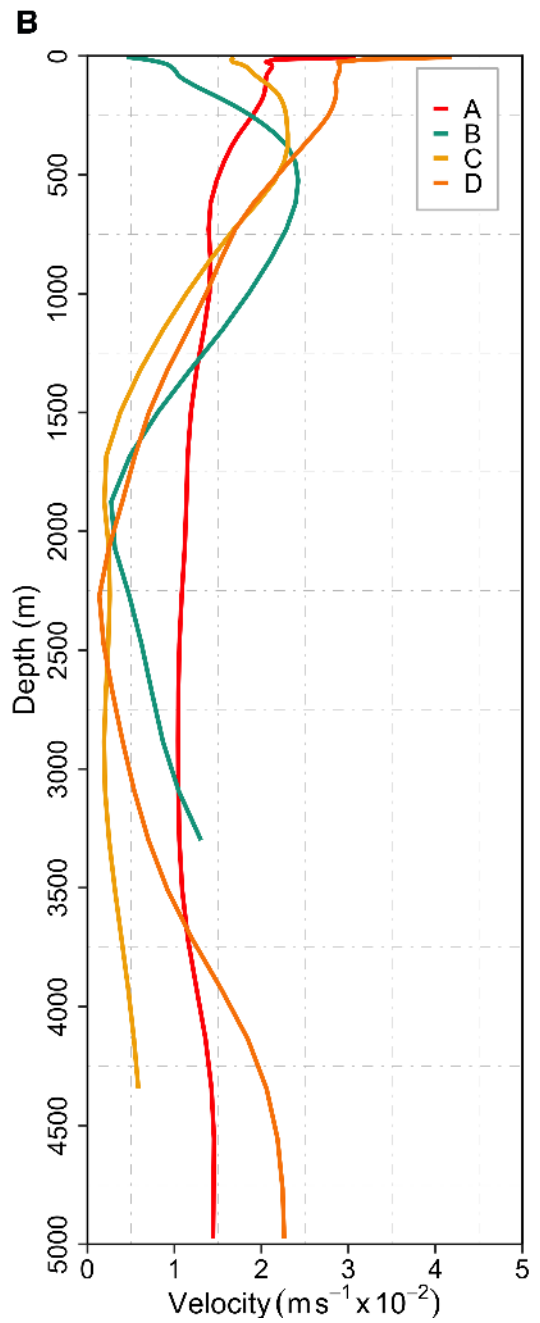
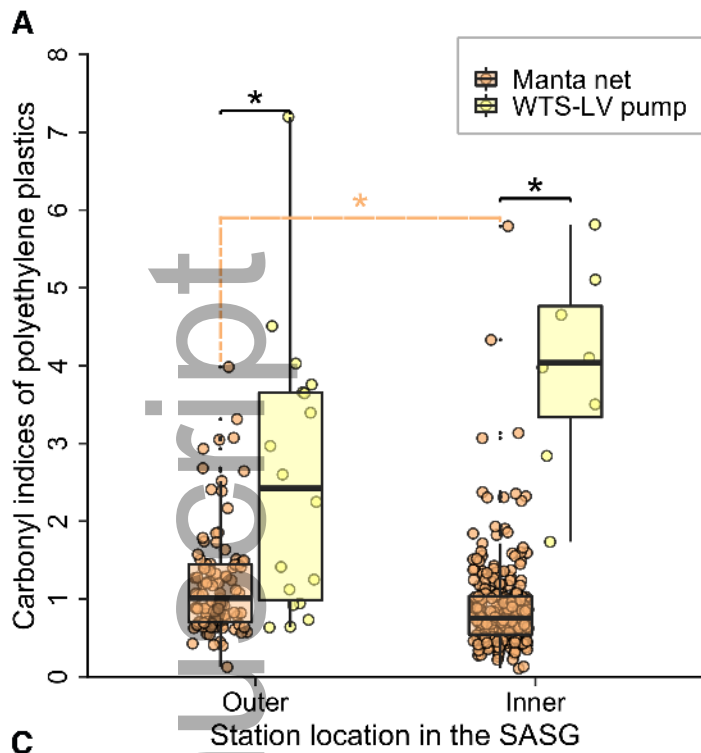
Author Manuscript



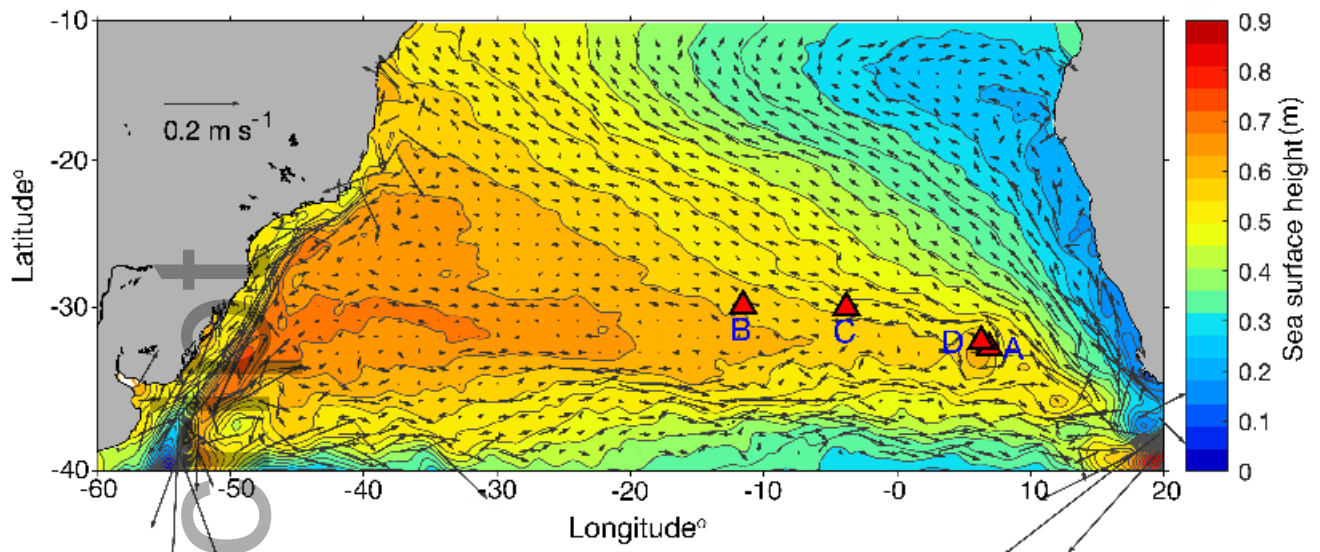
gcb_16089_f2.tif



gcb_16089_f3.tif



gcb_16089_f4.tif



Author Manuscript